2823

# Error Analysis and Numerical Tests for the Approximation of Unsteady Incompressible Viscous Flow by means of Projection Methods

**Jean-Luc Guermond** [1] and **Christian Tenaud** [2]

**Abstract.** This paper is concerned with the implementation of spatially discrete versions of Chorin–Temam's projection methods. The emphasis is put on the projection step, which enforces incompressibility. Three types of variational approximations are reviewed. Unconditional error estimates of order one and conditional error estimates of order two are given. Numerical simulations confirm these estimates. The effectiveness and accuracy of a projection algorithm is tested by comparing it with a Uzawa technique. Numerical tests on the driven cavity problem at high Reynolds numbers are reported.

## 1 INTRODUCTION

This paper is concerned with approximation properties of a class of fractional step techniques known as Chorin–Temam projection methods [3] [17]. These techniques have been proposed for approximating in time the unsteady incompressible Navier–Stokes equations. They are devised to avoid the coupling between the pressure and the velocity that is implied by the incompressibility constraint: div$u$=0. The basic idea consists in devising time marching procedures that uncouple viscous and incompressibility effects; the consequence of this splitting being that at each time step an otherwise hard-to-solve generalized Stokes problem is replaced by two simpler problems. These techniques are very efficient and have probably "been the first numerical schemes enabling a cost-effective solution of three-dimensional time-dependent problems" ( *cf.* Quartapelle [13, p. 177]). Although these techniques have long been used for calculating steady-state solutions to Navier–Stokes equations, they are now regaining their status as true time marching procedures for calculating time-dependent incompressible viscous flows. Their simplicity and efficiency render them particularly attractive to the CFD community (see *e.g.* [2], [4], [6], [7], [12], [14], [19]). This renewed interest for time-dependent solutions to Navier–Stokes equations is prompted by the increasing capacities of computers and the success of large eddy theories which recognize that unsteadiness of large eddies should be well predicted whereas smaller scales can (reasonably) be filtered.

Since its initial appearance, the projection method has been implemented with various types of spatial approximations and the fractional steps have been modified in order to improve the overall accuracy of the scheme. Though the stability of this method and its modified versions can generally be proven quite easily when space variables are continuous (see *eg.* [8] [15] [16]), the stability and convergence of their discrete counterparts are often overlooked in the literature (see *eg.* [7] [18] for a review on these problems).

This paper is organized as follows. In §2, we analyze three discrete projection schemes. For the first one the provisional velocity and the corrected one are approximated in the same space; that is, the corrected velocity satisfies a Dirichlet condition. This scheme is shown to be efficient for finite element approximations. In the second scheme, only the normal component of the end-of-step velocity is constrained. In the third algorithm, the projection step is formulated as a Poisson problem supplemented with a Neumann boundary condition. This technique is probably the easiest to implement, for it avoids a mass matrix problem that plagues the two others. In §3, we present numerical tests that demonstrate that projections schemes achieve second order accuracy at a lower cost than the classical Uzawa technique. In §4 numerical tests on the driven cavity are reported.

## 2 THE DISCRETE PROJECTION

### 2.1 Three possible schemes

Let $X$ and $M$ be respectively internal stable and convergent approximations of $\mathbf{H}_0^1(\Omega)$ et $\mathrm{L}^2(\Omega)/\mathbb{R}$. Let $A_X$:$X \longrightarrow X'$ so that $(A_X v,w)=(\nabla v,\nabla w)$ and $B_X$:$X \longrightarrow M \equiv M'$ so that $(B_X v,q)=(-\mathrm{div}v,q)$. $B_X$ is not systematically assumed to be onto. In order to simplify the presentation we assume that the convective non-linear terms in the Navier–Stokes equations have been linearized and we are interested in time approximations of the following model problem by means of fractional step techniques: for $f \in \mathrm{L}^2(0,T,X')$ and $v_0 \in \ker(B_X)$, find

[1] Laboratoire d'Informatique et de Mécanique pour les Sciences de l'Ingénieur (CNRS, UPR 3251), BP 133, F-91403 Orsay Cdex
[2] Laboratoire d'Informatique et de Mécanique pour les Sciences de l'Ingénieur (CNRS, UPR 3251), BP 133, F-91403 Orsay Cdex


*Computational Fluid Dynamics '94*
Published in 1994 by John Wiley & Sons Ltd

$u \in L^2(0,T;X)$ and $p \in L^2(0,T;M)$ so that

$$\begin{cases} \frac{du}{dt} + A_X u + B_X^t p = f \\ B_X u = 0 \\ u_{|t=0} = v_0 \end{cases} \tag{2.1}$$

If $B_X$ is onto, a possible scheme consists in approximating the predicted (viscous) and the corrected (projected) velocities in the same space, namely $X$. The prediction (diffusion) step is: find $\tilde{u}_{k+1} \in X$ so that

$$\frac{\tilde{u}_{k+1} - u_k}{\delta t} + A_X \tilde{u}_{k+1} = f_{k+1} - B_X^t p_k. \tag{2.2}$$

The correction (projection) step reads: find $u_{k+1}$ in $X$ and $p_{k+1} - p_k$ in $M$ so that

$$\begin{cases} \frac{u_{k+1} - \tilde{u}_{k+1}}{\delta t} + B_X^t (p_{k+1} - p_k) = 0 \\ B_X u_{k+1} = 0. \end{cases} \tag{2.3}$$

$B_X$ being onto, this problem is well posed. This algorithm is stable and convergent (*cf.* [9])); however, it may look paradoxical since $u_{k+1}$ satisfies $u_{k+1|\partial\Omega} = 0$ and the test functions of the projection step satisfy $v_{h|\partial\Omega} = 0$, whereas it may seem more appropriate to enforce only $u_{k+1} \cdot n_{|\partial\Omega} = 0$ and $v_h \cdot n_{|\partial\Omega} = 0$ as in the contiuous case. This choice has some consequence on the conditioning of the pressure operator $B_X B_X^t$; indeed, it can be shown that in the framework of finite element approximations based on regular triangulations of mesh size $h$, the condition number of the pressure operator is bounded from above as follows

$$\kappa(B_X B_X^t) \leq \frac{c}{\beta_X^2 h^2}, \tag{2.4}$$

where $\beta_X$ is the stability constant of $B_X^t$ (*ie.* the "inf-sup" constant). This bound shows that this scheme, though seemingly paradoxical, is optimal in terms of condition number of the pressure operator, since the underlying continuous problem is a Poisson equation supplemented with a homogeneous boundary condition whose discrete counterpart yields a condition number of order $1/h^2$. Hence, this scheme is adapted to finite element approximations. This conclusion is no longer valid for spectral approximations, since in these frameworks the stability constants of the operators $B_X^t$ tend to zero as the polynomial degree of the approximations increase; this phenomenon yields non optimal condition numbers for $B_X B_X^t$.

In order to cure this problem we introduce a velocity vector space so that the test functions satisfy $v.n_{|\partial\Omega} = 0$. Let $Y$ be a stable, convergent, and internal approximation of $H_0^{div}(\Omega) = \{v \in L^2(\Omega), \text{div} v \in L^2(\Omega), v \cdot n_{|\partial\Omega} = 0\}$. Assume also that $X \subset Y$ and define the orthogonal projection (in the sense of the duality induced by $L^2(\Omega)$) $\pi: Y' \longrightarrow X'$. Likewise we define, $B_Y$, the extension of $B_X$ so that $\pi B_Y^t = B_X^t$, and we assume that this extension is onto. In this framework, the diffusion step reads: look for $\tilde{u}_k \in X$ so that

$$\frac{\tilde{u}_{k+1} - \pi u_k}{\delta t} + A_X \tilde{u}_{k+1} = f_{k+1} - B_X^t p_k. \tag{2.5}$$

Note that $u_k$ must be projected onto $X'$ for this velocity does not naturally belong to $X$. The projection step consists of: look for $u_k \in Y$ et $(p_{k+1} - p_k) \in M$ so that

$$\begin{cases} \frac{u_{k+1} - \tilde{u}_{k+1}}{\delta t} + B_Y^t (p_{k+1} - p_k) = 0 \\ B_Y u_{k+1} = 0. \end{cases} \tag{2.6}$$

Thanks to the surjectivity of $B_Y$, this problem is well posed. It is possible to build spectral approximations falling in this functional framework so that the condition number of the pressure operator $B_Y B_Y^t$ is optimal (see [1] and [9] for other details). This algorithm has the same stability and convergence properties (*cf.* [9]) as the previous one; however, it is somewhat less cost-effective, for it requires to build two gradient operators, $B_X^t$ and $B_Y^t$, instead of one. One special feature of this scheme is that it does not explicitly require $B_X$ to be onto (*ie.* $B_X^t$ into and stable); indeed, the wellposedness of viscous step relies on the $X$-ellipticity of $A_X$ and that of the projection step relies on the surjectivity of $B_Y$. However, if $B_X^t$ is not into (*ie.* has spurious modes), it can be shown that the global stability in time on the pressure is ensured only on the component of the pressure that is orthogonal to the possible spurious modes of $B_X^t$ (after all, it is not surprising since uniqueness of the pressure that is solution to (2.1) is ensured only in $N(B_X^t)^\perp$).

The two methods presented above share the same drawback when it comes to implement them on computers. Indeed, once bases of $X$ (or $Y$) and $M$ are chosen, the projection step (2.3) or (2.6) is equivalent to solve the following linear system

$$B_h I_h^{-1} B_h^t (P_{k+1} - P_k) = \frac{B_h \tilde{U}_{k+1}}{\delta t}. \tag{2.7}$$

where $B_h$ is the matrix counterpart of either the operator $B_X$ or $B_Y$, and $U$, $P$ are the vectors of the components of $u$ and $p$ in the bases in question. Hence, the two methods presented above involve the inverse of the mass matrix $I_h$. If this matrix is not diagonal, which is the the case for finite elements, the projection step may become a not so easy problem to solve contrary to what we assumed. This difficulty leads to consider a third algorithm based on the representation of the projection step as a Poisson equation supplemented with a Neumann boundary condition.

For this purpose, introduce $Z$ a stable, convergent, and internal approximation of $H^1(\Omega)/\mathbb{R}$ (of finite dimension). Let $A_Z: Z \longrightarrow Z'$ be so that $(A_Z p, q) = (\nabla p, \nabla q)$. Set $M = Z$ in terms of vector space and equip $M$ with the norm of $L^2(\Omega)$ (*ie.* in some sense $M$ may be viewed as the completion of $Z$ in $L^2(\Omega)$). Introduce also the orthogonal projection $\pi: L^2(\Omega) \longrightarrow X'$. In this functional framework, the diffusion step is put into the form: look for $\tilde{u}_{k+1}$ in $X$ so that

$$\frac{\tilde{u}_{k+1} - \pi u_k}{\delta t} + A_X \tilde{u}_{k+1} = f_{k+1} - B_X^t p_k. \tag{2.8}$$

Note that $u_k$ must be projected onto $X'$. Then, look for $(p_{k+1} - p_k) \in Z$ so that

$$A_Z (p_{k+1} - p_k) = \frac{B_X \tilde{u}_{k+1}}{\delta t}. \tag{2.9}$$

This problem is weel-posed thanks to the $Z$-ellipticity of $A_Z$. Finally, the velocity is corrected (projected) as follows

$$u_{k+1}=\tilde{u}_{k+1} - \delta t\nabla(p_{k+1} - p_k). \qquad (2.10)$$

where the equation is understood in $\mathbf{L}^2(\Omega)$. This velocity is strictly divergence free, but it can be shown that its divergence tends (in some weak sense) to zero as the mesh is refined. This algorithm has the same stability and convergence properties as the two others, but it is far easier to implement. Note that, like the second algorithm, this algorithm does not require $B_X^t$ to be onto; likewise, the global stability in time on the pressure is ensured on the component that is orthogonal to the possible spurious modes of $B_X^t$.

## 2.2 Convergence estimates

For the three algorithms presented above, define the error functions: $e_k=u(t^k) - u_k$, $\tilde{e}_k=u(t^k) - \tilde{u}_k$, and $\delta_k=p(t^k) - p_k$, where $(u(t),p(t))$ is solution to (2.1). Let $L=X$ (in terms of vector space) and equip $L$ with the norme of $\mathbf{L}^2(\Omega)$. Introduce $M^1=M$ (in terms of vector space) and equip this space with the graph norm of one of the following discrete gradient $B_X^t$, $B_Y^t$, or $\pi\nabla$. For the three algorithms we can prove

**Theorem 1** *If the solution to (2.1) satisfies $u_{tt} \in L^2(0,T;L)$, $p_t \in L^2(0,T;M^1)$ and $|e_0|_L \le c\delta t$, $|\delta_0|_{M_1} \le c$ then:*

$$\sup_{0\le k\le K}\left[|e_k|_L^2 + \delta t^2|\delta_k|_{M^1}^2\right] + 2\alpha\delta t\sum_{l=1}^{K}|\tilde{e}_l|_X^2 \le c\delta t^2 \qquad (2.11)$$

The estimate (2.11) does not yield a strong result for the error on the pressure. In order to obtain a better estimate in $l^2(t^0,\dots,t^K;M)$, subtract (diffusion step) + $\pi$(projection step) from (2.1) and obtain:

$$B_X^t\delta_{k+1}=R_k - \frac{\pi e_{k+1} - \pi e_k}{\delta t} - A_X\tilde{e}_{k+1} \qquad (2.12)$$

where $R_k$ is the integral Taylor residual. Since (2.11) yields an estimate of $A_X\tilde{e}_{k+1}$ in $l^2(t^0,\dots,t^K;X')$ and $R_k$ is easily bounded from above, an error estimate on the pressure can be obtained if we can bound from above the ratio $(e_{k+1} - e_k)/\delta t$ in $l^\infty(t^0,\dots,t^K;L)$. The desired bound is given by

**Corollary 1** *If the solution to (2.1) is so that $u_{ttt} \in L^2(0,T;L)$ and $p_{tt} \in L^2(0,T;M^1)$ and if the data satisfy $|e_0|_L \le c\delta t^2$ and $|\delta_0|_{M_1} \le c\delta t$ then*

$$\sup_{0\le k\le K-1}\left[|e_{k+1} - e_k|_L^2 + \delta t^2|\delta_{k+1} - \delta_k|_{M^1}^2\right] \qquad (2.13)$$
$$+2\alpha\delta t\sum_{l=1}^{K-1}|\tilde{e}_{l+1} - \tilde{e}_l|_X^2 \le c\delta t^4$$

To prove this result, subtract two consecutive diffusion steps and repeat the process for two consecutive projection steps. The general structure of the resulting sytem of equations is unchanged, and one can apply theorem 1. If $B_X$ is not onto, introduce $\hat{M}=\ker(B_X^t)^\perp$, define $\hat{\pi}:M \longrightarrow \hat{M}$ the corresponding orthogonal projection, and denote by $\hat{\beta}_X$ the stability constant of $B_X^t\hat{\pi}$. Now we can prove

**Theorem 2** *Under the hypotheses of corollary 1, the error on the presure satisfies:*

$$\left[\delta t\sum_{0}^{K}|\hat{\pi}\delta_k|_M^2\right]^{1/2} \le \frac{c}{\hat{\beta}_X}\delta t \qquad (2.14)$$

This error estimate is a consequence of the stability of $B_X^t\hat{\pi}$ and of (2.12), (2.11), (2.13). The error estimate (2.13), which plays an important role here, means that $(u_{k+1}-u_k)/\delta t$ is a first order approximation of $\mathrm{d}u(t^{k+1})/\mathrm{d}t$ (as one should expect). Note that this estimate requires some regularity on $u_{ttt}$ and $p_{tt}$ whereas the error estimates on the velocity required some regularity only on $u_{tt}$ and $p_t$.

## 2.3 Higher orders

In order to improve the accuracy order of the method, Van Kan [19] proposed to use a Crank–Nicolson's scheme for the diffusion step:

$$\frac{\tilde{u}_{k+1} - \pi u_k}{\delta t} + \frac{1}{2}A_X(\tilde{u}_{k+1} + \tilde{u}_k)=f_{k+1/2} - B_X^t p_{k-1/2} \qquad (2.15)$$

As before, we can prove that the modified scheme is unconditionally first order accurate, and assuming that $A_X \in \mathcal{L}(L,L)$, which is always the case for discrete approximations, we have

**Theorem 3** *Let $Q=\sup_{v\in L}|A_Xv|_L/|v|_L$. If $u_{ttt}$ and $A_Xu_{tt}$ are in $L^2(0,T;L)$, $p_{tt} \in L^2(0,T;M^1)$, $\max(|e_0|_L,\delta t^{1/2}|\tilde{e}_0|_X,\delta t|\delta_{-1/2}|_{M^1}) \le c\delta t^2$ and if $\delta t \le 1/2Q$ then*

$$\sup_{0\le t^k\le T}\left[|e_k|_L + |\tilde{e}_k|_X\right] + \delta t\sum_{l=1}^{K}|\delta_{l-1/2}|_M^2]^{1/2} \le c(Q)\delta t^2 \qquad (2.16)$$

Of course, equivalent results can be proved for the backward three-level Euler algorithm.

$$\frac{3\tilde{u}_{k+1} - \tilde{u}_k - 3\pi u_k + \pi u_{k-1}}{2\delta t} + A_X\tilde{u}_{k+1}=f_{k+1} - B_X^t p_k \qquad (2.17)$$

# 3 NUMERICAL TESTS

## 3.1 Presentation of the method

In order to illustrate the efficiency of projection methods on a real Navier–Stokes problem, we have tested it on the driven cavity problem. Let $\Omega=]0,1[\times]0,1[$ and define on $\Omega$ a uniform staggered mesh-and-cell grid (MAC) introduced by Harlow and Welch [10]. One nice feature of the MAC approximation is that it is easily interpretable in terms of finite differences and fits also into a variational framework.

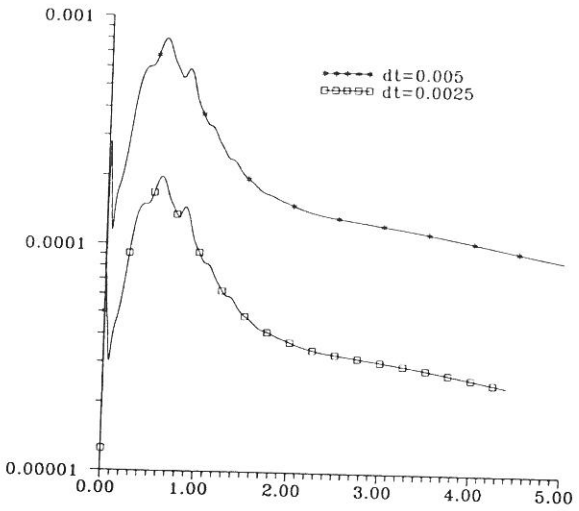


**Figure 1.** Error on the velocity given by the projection scheme as a function of the physical time. The reference solution is obtained by Uzawa iterations. The driven cavity problem, $R_e$=3200.

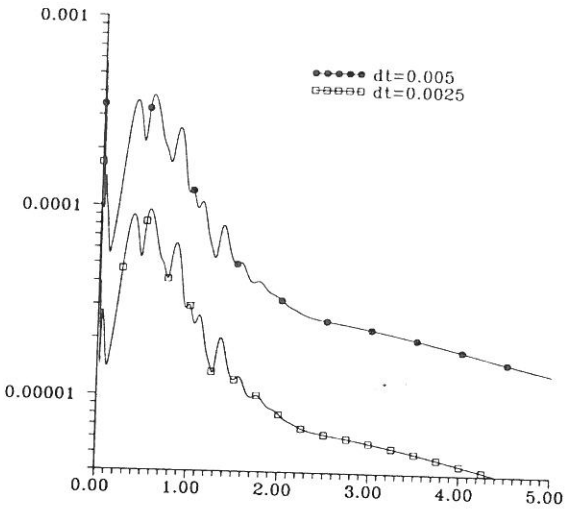


**Figure 2.** Error on the pressure given by the projection scheme as a function of the physical time. The reference solution is obtained by Uzawa iterations. The driven cavity problem, $R_e$=3200.

The time derivative in the diffusion step is approximated by means of a Crank–Nicolson scheme (Van Kan's approach) and the non-linear term is linearized and implicited as follows

$$u.\nabla u(t^{k+1}) = \frac{1}{2}(3u_k - u_{k-1}).\nabla u_{k+1} + O(\delta t^2). \qquad (3.18)$$

In the particular framework of the MAC approximation the three projection steps as described above are equivalent, for the mass matrix is diagonal and the operator $B_Y B_Y^t$ coincides with the approximation of the Laplace operator supplemented with the homogeneous Neumann boundary condition.

## 3.2 Accuracy tests

In order to test the accuracy of the projection algorithm we have compared the pressure and the velocity field that it gives at each time step with the exact solution of the coupled problem. The so-called exact solution is obtained by solving the pressure equation involving the Uzawa operator by means of a preconditioned gradient technique, the preconditioner being the Laplace operator supplemented with the homogeneous Neumann boundary condition.

The tests are performed for $0 < t \leq 5$.. The driving condition (*ie.* $u$=1 on the upper face of the cavity) is regularized for $0 < t \leq 0.1$. The Reynolds number is set to 3200. The tests have been carried out with two times steps: $\delta t$=0.005 and $\delta t$=0.0025. The results are reported in figures 1 and 2. The base 10 logarithm of the error in velocity and pressure plotted as a function of the physical time. Note that second order accuracy is obtained for the velocity and the pressure.

## 3.3 Tests on the CPU time

In order to illustrate the cost-effectiveness of projection methods for approximating time-dependent Navier-Stokes equations we have reported the cumulated CPU time (in second on a CRAY C98) as a function of the physical time in figures 3 and 4. The test problem is the driven cavity at $R_e$=3200 with a 65 × 65 mesh. Note the linear dependence of the CPU time with respect to the physical time for the projection method (see figure 4). The number of iterations required by the Uzawa technique to reach a fixed level of accuracy depends on the unsteadiness of the problem; as a result, the relation between the CPU time and the physical time is not exactly linear (see figure 3). In the present case the Uzawa based algorithm is 30 times slower than the projection technique. Some numerical unstabilities have been observed in the Uzawa program if the number of Uzawa iterations or the accuracy threshold are relaxed in order to lower the computational cost. This example clearly demonstrates that projection techniques make a near optimal balance between accuracy and cost-effectiveness. Though the Uzawa technique is optimal for solving steady-state Stokes problems, it should not be recommanded for solving time-dependent Navier–Stokes problem.

# 4 THE DRIVEN CAVITY PROBLEM

To illustrate the capability of the code to solve real configuration, that is to say moderate-to-high Reynolds number flows, it is tested on the well known two-dimensional driven cavity problem. In what follows, the Reynolds number, based on the grid-spacing, is high enough te be sure that, using central differences for the discretization of the convective terms, the

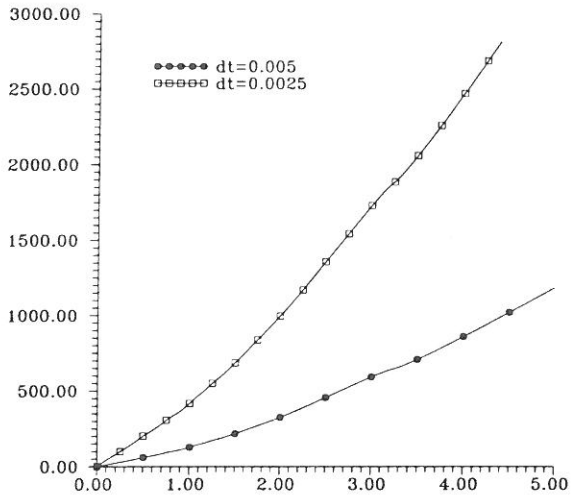


**Figure 3.** Uzawa technique: CPU time vs. physical time. The driven cavity problem, $R_e$=3200, 65 × 65 mesh.

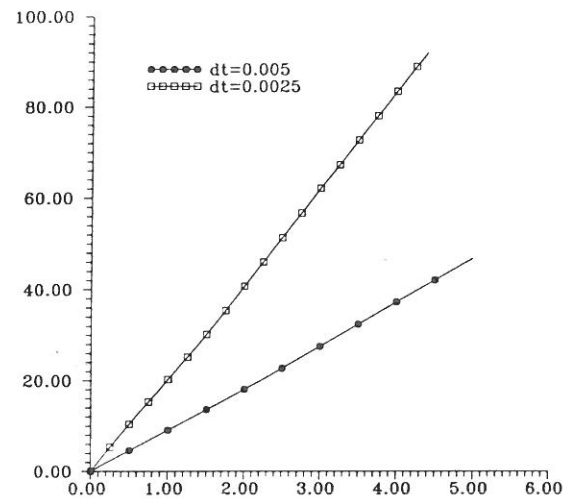


**Figure 4.** Projection algorithm: CPU time vs. physical time. The driven cavity problem, $R_e$=3200, 65 × 65 mesh.

calculation stays unstable. Therefore, an upwind differences are applied for the space derivatives of the convective terms.

## 4.1 Numerical scheme

The numerical scheme used is an upwind Total-Variation-Diminishing (TVD) scheme originally developped by Harten [11] and modified by Yee [20]. It is generally employed for the computation of compressible applications. This specific scheme has however been chosen since it uses function which controles the numerical diffusion to ensure very small one. The momentum equations in $x$ and $y$ direction are solved separately ; therefore we could consider a set of two scalar independent equations. Regarding the non-linear terms of the convection, we suppose that the characteristic speeds are respectively $u$ and $v$ in the $x$ and $y$ directions. As for moderate-to-high Reynolds number flows there exits unsteady phenomena, we need time-accurate calculations. Therefore, the scheme apply on the convective terms is an explicit scheme which is second order accurate in time.

If we consider a grid point where $x_i$=$i.\Delta x$ and $y_j$=$j.\Delta y$, the convective terms of the projection in the $x$ direction of the momentum equation are written as follows :

$$\left(u\frac{\partial u}{\partial x}\right)_{i,j} = \frac{1.}{2\,\Delta x}\left[u_{i,j}\left(u_{i+1,j}-u_{i-1,j}\right)+\Phi_{x_{i+1/2,j}}-\Phi_{x_{i-1/2,j}}\right]$$

$$\left(v\frac{\partial u}{\partial y}\right)_{i,j} = \frac{1.}{2\,\Delta y}\left[v_{i,j}\left(u_{i,j+1}-u_{i,j-1}\right)+\Phi_{y_{i,j+1/2}}-\Phi_{y_{i,j-1/2}}\right]$$

Where the diffusive flux functions $\Phi$ stand for a correction added to the central differences. In order to ensure that the present scheme is a second order upwind TVD scheme, the $\Phi$ functions in the $x$ direction are written following :

$$\Phi_{x_{i+1/2,j}}=\sigma\left(u_{i,j}\right)\left(\xi_{i+1,j}+\xi_{i,j}\right)-\left|u_{i,j}+\sigma\left(u_{i,j}\right)\gamma_{i+1/2,j}\right|\alpha_{i+1/2,j}$$

$$\Phi_{x_{i-1/2,j}}=\sigma\left(u_{i,j}\right)\left(\xi_{i,j}+\xi_{i-1,j}\right)-\left|u_{i,j}+\sigma\left(u_{i,j}\right)\gamma_{i-1/2,j}\right|\alpha_{i-1/2,j}$$

where $\alpha_{i+1/2,j}=\left(u_{i+1,j}-u_{i,j}\right)$ stands for the forward difference of the local charcateristic variables in the $x$ direction and

$$\sigma(z)=\frac{1}{2}\left(|z|-\frac{\Delta t}{\Delta x}z^2\right)$$

$$\gamma_{i+1/2,j}=\begin{cases}\left(\xi_{i+1,j}-\xi_{i,j}\right)/\alpha_{i+1/2,j} & \text{if} \quad \alpha_{i+1/2,j}\neq 0.\\ 0. & \text{if} \quad \alpha_{i+1/2,j}=0.\end{cases}$$

The limitor function $\xi$, which acts as an anti-diffusive flux, is expressed using the "Super-Bee" formulation [21]. This formulation has been chosen since it gives less numerical diffusion than other classical functions found in the litterature [21] [22]:

$$\xi_{i,j}=S.\max\left\{0.,\min\left(2.\left|\alpha_{i+1/2,j}\right|,S.\alpha_{i-1/2,j}\right),\ \min\left(\left|\alpha_{i+1/2,j}\right|,2.S.\alpha_{i-1/2,j}\right)\right\}$$

where $S$=$sgn\left(\alpha_{i+1/2,j}\right)$

Similar formulations as in streamwise direction are used to express the numerical flux functions in the $y$ direction.

## 4.2 Numerical results

The numerical code based on the upwind TVD scheme is first checked on the calculation of the driven cavity at rather low Reynolds number, for instance $Re$=3200, for which steady solution must be obtained. The grid has 65 points in both $x$ and $y$ directions. The time step employed is $\Delta t$=5. $10^{-3}$ which leads to a $CFL$ number close to 0.32. The calculation is performed up to a dimensionless time equal to $T$=150.. On the figure 5, we plot the evolution of the longitudinal velocity ($u$) versus the normal direction ($y$) at the midd-line $x$=1/2, while

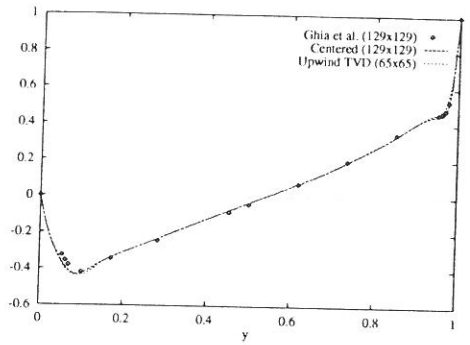


**Figure 5.** The driven cavity problem, $R_e$=3200.: profiles of the longitudinal velocity $u$ versus the normal coordinate $y$ at the midd-position of the cavity ($x$=1/2).

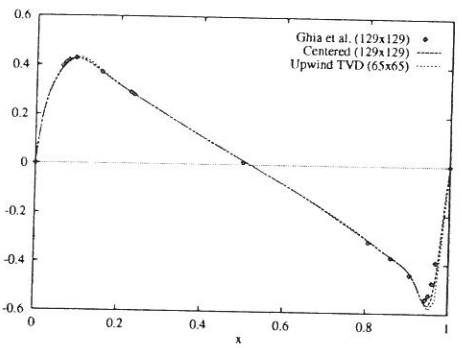


**Figure 6.** The driven cavity problem, $R_e$=3200.: profiles of the vertical velocity $v$ versus the longitudinal coordinate $x$ at the midd-position of the cavity ($y$=1/2).

the longitudinal evolution of the vertical velocity ($v$) at the midd-line $y$=1/2 is presented on the figure 6. The numerical results obtained through the use of the upwind TVD scheme are compared with the numerical results (dots) obtained over a (129x129) grid by Ghia et al. [5] using a steady-state approach. As the Reynolds number is moderate, the present results are also compared with the solution obtained with an implicit centered scheme as spatial discretization of the convective terms, using 129 grid-points in each direction. Rather good agreements for both $u$ and $v$ profiles are achieved compared, on one hand, with the steady-state solution [5] and, on the other hand, with the solution using centered differences. Nevertheless, very close to the extrema of the curve, some slight discrepancies could be seen on the profiles obtained by using the upwind TVD scheme. These discrepancies might be due to the use of a too coarse grid in these regions; finer grid must be employed to get better results.

Secondly, the problem of the driven cavity at a Reynolds number equal to $10^4$ has been undertaken. The mesh size is (256x256) points in ($xxy$) directions; the time step is $\Delta t$=1.5 $10^{-3}$ which corresponds to $CFL$=0.38. The calculation is carried out for $0 < t \leq 24.$. The driving condition ($u$=1.) is applied on the upper surface of the cavity and regularized for $0 < t \leq 0.1$. On figures 7, 8, 9, 10, 11, 12, we can see the time-evolution of the vorticity isovalues ($t$=0. refers to the initial condition). Up to the dimensionless time equal to $t$=14., a important vortex of negative magnitude grows and takes place over a large extent, close to the center of the cavity. At this moment ($t$=14.), a secondary vortex with a positive intensity is created close to the upper surface of the cavity (figure 7). Following that time, a second vortex ($t$=16., see figure 8) and a third one ($t$=18., see figure 9) are generated on the left part of the cavity. These three secondary structures are convected at the perimeter of the main vortex. The magnitude of the convective velocity depends on the interaction between these secondary vorticies and the main structure. As the convective velocity of the third vortex seems to be greater than the velocity of the second one, these two structures merge together at $t$=20. (figure 10) and collapse into a more extended vortex (figure 11). At $t$=20., a fourth stucture is then created close to the lower-left corner of the cavity (figure 10). Finally, the processus seems to continue (figures 11 12). Several coherent structures with a positive circulation are generated. They are located at the perimeter of the main negative vortex situated over a large extent.

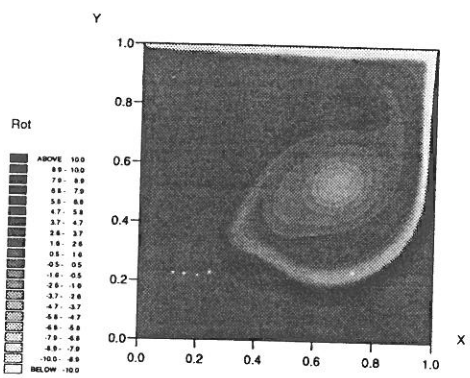


**Figure 7.** The driven cavity problem, $R_e$=$10^4$: the isovalues of the vorticity at $t$=14.

## 5 CONCLUSION

This paper is concerned with the implementation of spatially discrete versions of Chorin–Temam's projection methods. The emphasis is put on the projection step, which enforces incompressibility.

Three types of variational approximations of Chorin–Temam's projection methods have been presented. In the first one, the projection step is solved as a div-grad problem with velocity test functions satisfying a (at first glance) paradoxical Dirichlet condition. In the second method, the projection step is still

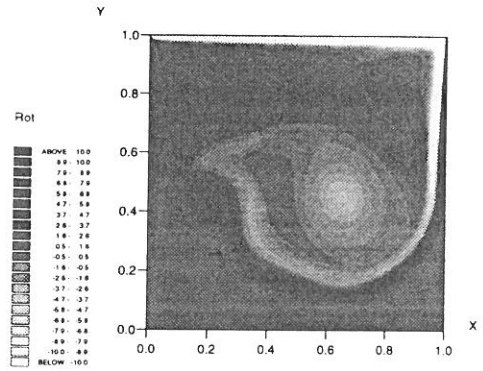


**Figure 8.** The driven cavity problem, $R_e$=$10^4$: the isovalues of the vorticity at $t$=16.

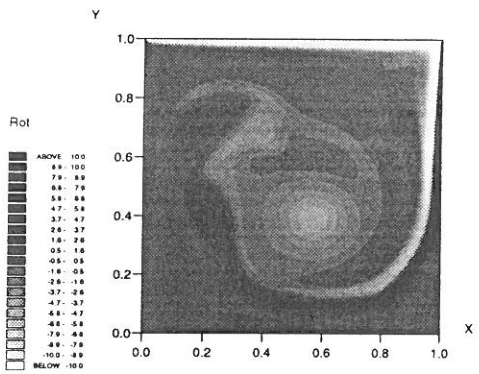


**Figure 9.** The driven cavity problem, $R_e$=$10^4$: the isovalues of the vorticity at $t$=18.

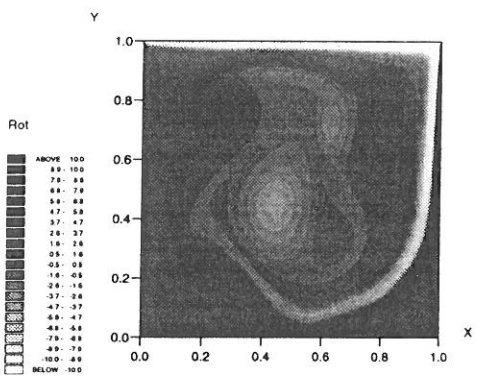


**Figure 10.** The driven cavity problem, $R_e$=$10^4$: the isovalues of the vorticity at $t$=20.

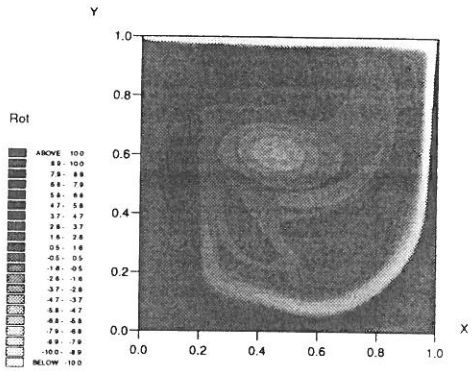


**Figure 11.** The driven cavity problem, $R_e$=$10^4$: the isovalues of the vorticity at $t$=22.

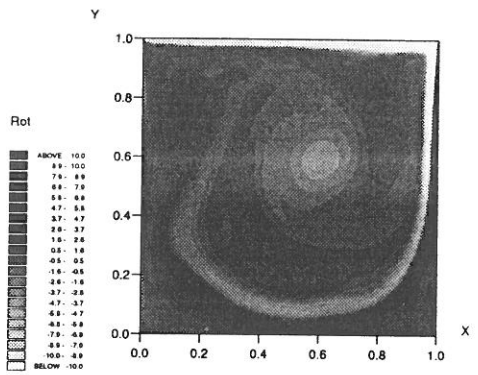


**Figure 12.** The driven cavity problem, $R_e$=$10^4$: the isovalues of the vorticity at $t$=24.

solved as a div-grad problem but the velocity test functions satisfy a boundary condition only for the normal component. In the third approach the projection step is solved in the form of a Poisson equation supplemented with a Neumann boundary condition. The first method is shown to be legitimate and economical for finite element approximations, whereas the second is shown to be useful also for spectral approximations. The third one is probably the easiest to implement since it avoids the problem of the mass matrix occurring in the two others. Though the second and third approaches do not directly involve a inf-sup condition, this condition is pointed out to be necessary to establish stability results and rule out possible spurious pressure. Finally, numerical tests on the driven cavity problem at high Reynolds number illustrate the cost-effctiveness and accuracy of the proposed algorithms. Two Reynolds number flows have been computed ($R_e$=3200. and $R_e$=$10^4$.). As these computations present moderate-to-high Reynolds numbers based on the grid spacing, an upwind differences using a Total-Variation-Diminishing (TVD) scheme are applied for the space derivatives of the convective terms of the momentum equation. This upwind TVD scheme was first checked on the calculation at a moderate Reynolds number ($Re$=3200); good results have been achieved, compared with those obtained by Ghia et al. [5] using a steady-state approach. The high Reynolds number calculation ($R_e$=$10^4$.) has then been undertaken. During the transient stage after a regularized starting, the formation of rotating structures within the flow has been analysed.

## ACKNOWLEDGEMENTS

The authors acknowledge helpful discussions with C. Bernardi, L. Quartapelle and P. Le Quéré. The computations have been carried out on the Cray C98 of IDRIS; the support of this institution is greatly acknowledged.

## REFERENCES

[1] M. Azaiez, C. Bernardi and M. Grundmann, Méthodes spectrales pour les équations du milieu poreux, R 93029, Laboratoire d'Analyse Numérique, Paris VI, 1993.

[2] J. B. Bell, P. Colella and H. M. Glaz, A second order projection method for the incompressible Navier–Stokes equations, *J. Comput. Phys.*, **85**, 1989, 257–283.

[3] A. Chorin, Numerical simulation of the Navier–Stokes equations, *Math. Comp.*, 22, 1968, 745–762.

[4] J. Donea, S. Giuliani, H. Laval, L. Quartapelle, Finite element solution of the unsteady Navier–Stokes equations by a fractional step method, *Comput. Meths. Appl. Mech. Engrg.*, **30**, 1982, 53–73.

[5] U. Ghia, K.N. Ghia, C.T. Shin , High-Re Solutions for incompressible Flow Using the Navier-Stokes Equations and a Multigrid Method, *J. Comput. Phys.*, **48**, 1982, 387–411.

[6] K. Goda, A multistep technique with implicit difference schemes for calculating two- or three-dimensional cavity flows, *J. Comput. Phys.*, **30**, 1979, 76–95.

[7] P. M. Gresho and S. T. Chan, On the theory of semi-implicit projection methods for viscous incompressible flow and its implementation via finite element method that also introduces a nearly consistent mass matrix. Part I and Part II, *Int. J. Numer. Methods Fluids*, **11**, 1990, 587–620.

[8] J.-L. Guermond, Remarques sur les méthodes de projection pour l'approximation des équations de Navier–Stokes, *Numer. Math.*, 1994, in press and LIMSI report 93-30.

[9] J.-L. Guermond, Some implementations of projection methods for Navier–Stokes equations, submitted to *Modél. Math. Anal. Numér.* ($M^2$AN) and LIMSI report 94-03.

[10] F.H. Harlow and F.E. Welch, Numerical calculation of time-dependent viscous incompressible flow of fluid with free surface, *Phys. Fluids*, **8**, 1965, 2182–2189.

[11] A. Harten, High Resolution Schemes for Hyperbolic Conservation Laws. *J. Comput. Phys.* **49**, 1983, 357–393.

[12] J. Kim and P. Moin, Application of a fractional-step method to incompressible Navier–Stokes equations, *J. Cumput. Phys.*, **59**, 1985, 308–323.

[13] L. Quartapelle, *Numerical solution of the incompressible Navier–Stokes equations*, ISNM **113**, Birkhäuser, Basel, 1993.

[14] M. Resenfeld, D. Kwak and M. Vinokur, A fractional step solution for the unsteady incompressible Navier–Stokes equations in generalized coordinate systems, *J. Comput. Phys.*, **94**, 1991, 102–137.

[15] J. Shen, On Error Estimates of Projection Methods for Navier–Stokes Equation: First-Order Schemes, *SIAM J. Numer. Anal.*, **29**, 1, 1992, 57–77.

[16] R. Temam, *Navier–Stokes Equations*, Studies in Mathematics and its Applications, 2, North-Holland, 1977.

[17] R. Temam, Une méthode d'approximation de la solution des équations de Navier–Stokes, *Bull. Soc. Math. France*, 98, 1968, 115–152.

[18] R. Temam, Remark on the pressure boundary condition for the projection method, *Theoret. Comput. Fluid Dynamics*, **3**, 1991, 181–184.

[19] J. Van Kan, A second-order accurate pressure-correction scheme for viscous incompressible flow, *SIAM J. Sci. Stat. Comput.*, **7**, 3, 1986, 870–891.

[20] H.C. Yee and A. Harten, Implicit TVD Schemes for Hyperbolic Conservation Laws in Curvilinear Coordinates. AIAA Jal., **25**, 2, 1987, 266–274.

[21] H.C. Yee, Construction of Explicit and Implicit Symmetric TVD Schemes and Their Applications, *J. Comput. Phys.*, **68**, 1987, 151–179.

[22] H.C. Yee, Numerical Experiments With a Symmetric High Resolution Shock-Capturing Scheme, NASA TM-88325, 1986

[23] N.N. Yanenko, *Fractional Steps Methods*, English translation, Springer Verlag, 1971.